GENE THERAPY

An AAV variant selected through NHP screens robustly transduces the brain and drives secreted protein expression in NHPs and mice

Luis Tecedor[1]†, Yong Hong Chen[1]†, David E. Leib[1,2]†, Paul T. Ranum[1,2]†, Megan S. Keiser[3], Brian C. Lewandowski[1], Elli M. Carrell[1], Elena Lysenko[1], Icnelia Huerta-Ocampo[1], Sakshi Arora[1], Congsheng Cheng[1], Xueyuan Liu[1], Beverly L. Davidson[1,4]*

Recent work has shown that prolonged expression of recombinant proteins after adeno-associated virus (AAV)–mediated delivery of gene therapy to long-lived, ventricle-lining ependymal cells can profoundly affect disease phenotypes in animal models of neurodegenerative diseases. Here, we performed in vivo screens of millions of peptide-modified capsid variants of AAV1, AAV2, and AAV9 parental serotypes in adult nonhuman primates (NHPs) to identify capsids with potent transduction of key brain tissues, including ependyma, after intracerebroventricular injection. Through these screens, we identified an AAV capsid, AAV-Ep$^+$, with markedly increased potency in transducing ependymal cells and cerebral neurons in NHPs. AAV-Ep$^+$'s potency was conserved in three species of NHP, two mouse strains, and human neurons derived from induced pluripotent stem cells. To apply AAV-Ep$^+$ to the treatment of ceroid lipofuscinosis type 2 disease, a lysosomal storage disorder caused by loss-of-function mutations in *tripeptidyl-peptidase 1* (*TPP1*), we used the capsid to package the human *TPP1* transgene (AAV-Ep$^+$.hTPP1) and delivered the construct by intracerebroventricular injection into mice lacking TPP1 activity. AAV-Ep$^+$ provided robust and therapeutically relevant TPP1 protein concentrations in these mice, significantly improving tremor and life span. In NHPs, high cerebrospinal fluid (CSF) TPP1 concentrations were achieved after intracerebroventricular delivery of AAV-Ep$^+$.hTPP1 at a total dose of 1×10^{12} viral genomes, which was more than 30× lower than previously reported doses in NHPs. These results suggest that AAV-Ep$^+$ may be a potent vector for gene therapy applications where CSF protein expression is required.

INTRODUCTION

Lysosomal storage disorders (LSDs) are genetic diseases that result from deficiencies in individual enzymes that break down carbohydrates or lipids, leading to accumulation of undigested substrates within cells (*1*). In many cases, the peripheral manifestations of these disorders can be addressed by enzyme replacement therapy (ERT) where the enzyme is periodically infused, generally biweekly or monthly, into the bloodstream for uptake by affected organs (*2*). Tissues that are difficult to treat in this manner include the brain, because ERT generally does not cross the blood-brain barrier. This can be overcome, in part, by direct infusion into the cerebrospinal fluid (CSF) through a chronically implanted device; however, periodic infusions require patients to live close to infusion centers, and the implanted device is prone to serious infections (*3*). The cross-correction properties of many lysosomal enzymes make them attractive candidates for gene therapy (*4*–*7*), because genetically corrected cells can synthesize and secrete product for uptake by other cells (*5*). Ependymal cells, the epithelial cells that line the ventricular spaces of the brain, provide an ideal site for secretion of recombinant proteins into the CSF for distribution throughout the brain, aided by perivascular spaces (*8*–*10*). One LSD for which cross-correction can be beneficial is ceroid lipofuscinosis type 2 (CLN2) disease, which is caused by recessively inherited mutations in *TPP1*, which encodes the enzyme tripeptidyl-peptidase 1. TPP1 is a soluble lysosomal hydrolase that, when absent, causes a debilitative and fatal childhood neurological disease (*11*). TPP1 is synthesized as a proenzyme that is activated to the holoenzyme at low pH in the lysosome. When overexpressed, the proenzyme is secreted and can enter nonexpressing cells by receptor-mediated endocytosis, resulting in cross-correction (*12*, *13*). Prior work in a canine model of CLN2 disease showed that TPP1 secretion from transduced ependyma could markedly extend life span and reduce symptoms through brain-wide biodistribution of the secreted product (*14*).

To translate this work clinically, we undertook screens to identify adeno-associated virus (AAV) capsid variants that effectively targeted ependymal cells for CSF distribution and transduced parenchymal neurons for enhanced effects. We developed capsid libraries based on a number of AAV serotypes, infused the library mix into wild-type, adult old world nonhuman primates (NHPs), and, after two rounds of enrichment, identified a lead candidate, AAV-Ep$^+$, that robustly transduced ependymal cells throughout the entire ventricular system. Moreover, AAV-Ep$^+$ transduced neurons throughout brain cortices and other brain regions, with similar transduction patterns in three different adult NHP species, in two mouse strains and in human neurons derived from induced pluripotent stem cells (iPSCs), demonstrating cross-species tropism. In NHPs, there was limited gene expression in sampled dorsal root ganglia, a common site of toxicity seen with AAV9-based vectors administered to the CSF (*15*).

When applied to a murine model of CLN2 disease, AAV-Ep$^+$.hTPP1 improved the disease phenotype and prolonged life span at doses

[1]Raymond G. Perelman Center for Cellular and Molecular Therapeutics, Children's Hospital of Philadelphia, Philadelphia, PA 19104, USA. [2]Latus Bio, Philadelphia, PA 19104, USA. [3]Department of Neurological Surgery, NeuroTech Institute, Ohio State University, Columbus, OH 43210 USA. [4]Department of Pathology and Laboratory Medicine, University of Pennsylvania, Philadelphia, PA 19104, USA.
*Corresponding author. Email: davidsonbl@chop.edu
†These authors contributed equally to this work.

lower than those used in previous publications using wild-type capsids. When evaluated in healthy NHPs, AAV-Ep$^+$.hTPP1 generated hTPP1 protein concentrations in CSF and parenchyma that were ninefold greater than in CSF from children without CLN2 disease, supporting the translatability of this approach for CLN2 disease gene therapy and other disorders that would benefit from steady-state protein delivery to the CSF.

RESULTS

Peptide-modified AAV library enrichment identifies capsid variants with high target tissue tropism

Capsids with improved tropism for ependymal cells and brain parenchyma were identified using a peptide-modified AAV capsid library screening approach (Fig. 1A). To increase capsid diversity, the screen included three different parental serotypes (AAV1, AAV2, and AAV9). Capsid sequences were modified by insertion of a random heptamer peptide into the variable region of loop 8 at amino acid positions 590, 587, and 588 for AAV1, AAV2, and AAV9, respectively. The three serotype libraries were pooled and injected into the lateral ventricle of an adult rhesus macaque (see table S1 for all NHP information). Brain regions of interest, including ependyma and cerebral cortices, were collected and a second-round AAV library was generated from the viral DNA recovered from the collected tissues. The newly prepared AAV library was injected into the lateral ventricle of a second adult rhesus macaque. Illumina amplicon sequencing was performed on tissues from the second round of screening and analyzed to assess capsid variant performance (fig. S1). After two rounds of selection, variants were evaluated on the basis of enrichment in ependyma and other brain regions. On the basis of this analysis, the four top-performing capsids were selected for fluorescence validation (two variants from serotype 2 and one variant each from serotypes 1 and 9; see Materials and Methods). These were independently produced and assessed for ependymal, cortical, and subcortical tropism (Fig. 1, B and C).

AAV candidate validation identifies a lead variant with broad cortical, subcortical, and ependymal transduction

The four capsid variants selected for broad enrichment across ependymal and parenchymal regions (AAV-Ep's) were packaged as single-stranded DNA genomes with four distinct fluorescent reporter transgenes driven by the ubiquitous CAG promoter. These reporters were selected on the basis of spectral compatibility and brightness to minimize potential biases on the fluorescence readout. All four capsid variants were produced and purified (see Materials and Methods) at titers greater than 5×10^{12} viral genomes (vg)/ml with total yields as expected for other similar research-grade virus preparations. The AAV variants were pooled and injected at a total dose of 4×10^{13} vg into the right anterior lateral ventricle of a single adult rhesus macaque (Fig. 2). After 3 weeks, the animal was euthanized, and tissues were processed for histology. Vector distribution was assessed using direct epifluorescence of the four reporter transgenes. Whereas AAV-Ep4 and AAV-Ep1 transduced ependyma in the lateral ventricle near the site of injection, only AAV-Ep1 (noted as AAV-Ep$^+$ in all subsequent uses) was

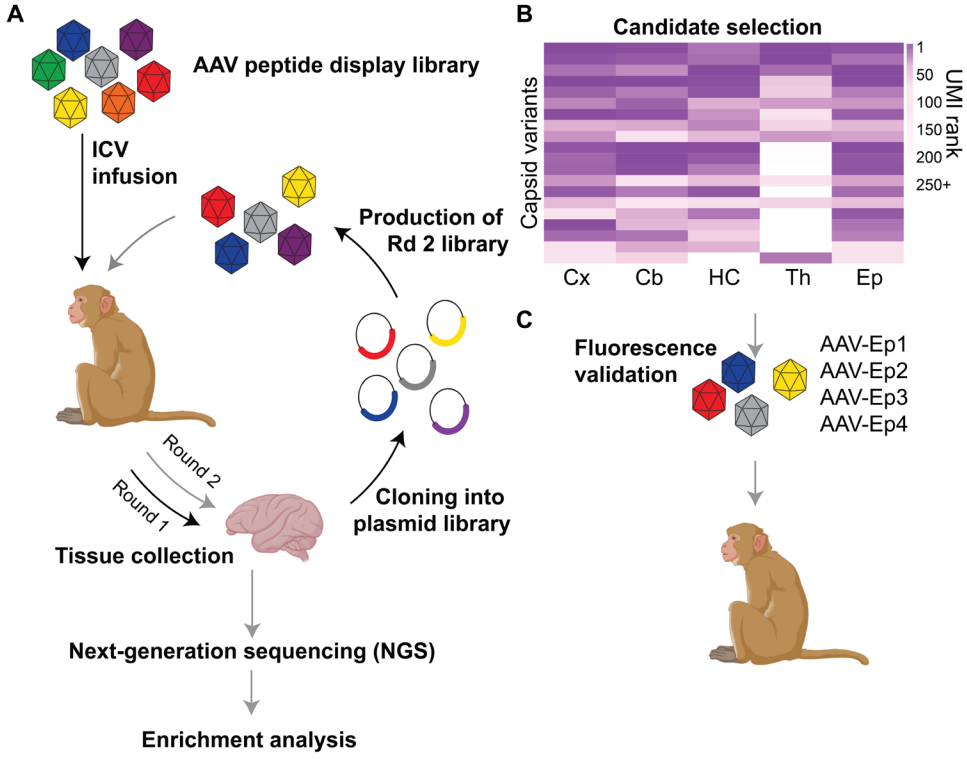

Fig. 1. AAV capsid library enrichment and candidate selection. (**A**) Schematic depicting the AAV capsid selection pipeline. AAV1, AAV2, and AAV9 libraries were generated that contained a semirandom heptapeptide insert within the variable region of loop 8, yielding an initial ~6.8 million capsid variants (1.3 million for AAV1-, 2.3 million for AAV2-, and 3.25 million for AAV9-based libraries). Variant enrichment was achieved by two sequential passages through a rhesus macaque brain. The first primate (black arrows) received a single intracerebroventricular infusion of the round one input library containing AAV capsid libraries from three parental serotypes. DNA extracted from collected tissues from the first animal and recovered AAV variant sequences were used to generate a round two AAV input library that was delivered by intracerebroventricular infusion into a second rhesus macaque from which both viral DNA and cellular RNA were collected. Successfully enriched capsids were identified using Illumina sequencing of viral amplicons. Capsid performance was assessed using a combination of total detection in target tissues and enrichment, which was defined as the ratio of a capsid's relative abundance in a target region versus the input library. (**B**) Exemplar heatmap showing AAV1 capsid variant abundance rankings for DNA data; rank 1 = highest UMI count (out of 7900 AAV1 variants above threshold in these regions). Cx, cerebral cortex; Cb, cerebellum; HC, hippocampus; Th, thalamus; Ep, ependyma. (**C**) Four highly enriched capsid variants were selected for fluorescence validation. Selected capsids expressing fluorescent payloads were individually cloned and produced, then pooled for subsequent validation. NHP images from (A) and (C) are from BioRender.com

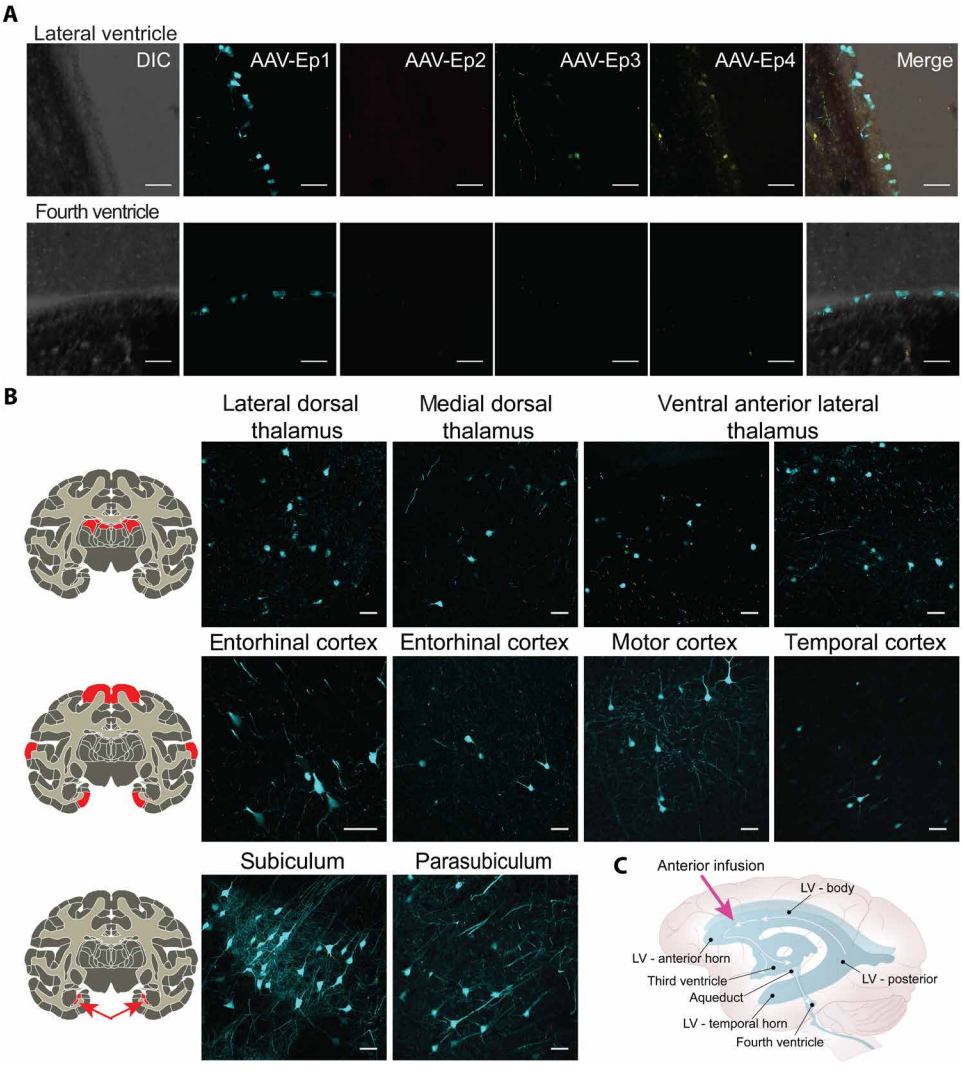

Fig. 2. AAV-Ep reporter evaluation. (**A**) Fluorescent reporter expression detection (see Materials and Methods) in the lateral (top) and fourth (bottom) ventricles of an adult rhesus macaque that received a unilateral intracerebroventricular infusion of the four top candidate capsids 4 weeks earlier. DIC (differential interference contrast microscopy), AAV-EP1 (AAV1 variant; CAG.mTFP1), AAV-Ep2 (AAV2 variant; CAG.mRuby3), AAV-Ep3 (AAV2 variant; CAG:mNG), and AAV-Ep4 (AAV9 variant; CAG:mTagBFP). (**B**) Fluorescent reporter expression for AAV-Ep1 in extra-ependymal regions of the same animal examined in (A). Scale bars, 50 μm. Coronal images are adapted from (*38*). (**C**) Depiction of the site of infusion (magenta arrow) into the right anterior lateral ventricle.

found in the more distant fourth ventricle (Fig. 2A). AAV-Ep$^+$ also transduced numerous cells in the cortex and deep brain regions, including the thalamus, subiculum, and parasubiculum (Fig. 2B). A comparison of capsid performance in sequenced tissues showed a 22-fold enrichment of AAV-Ep$^+$ against its parental capsid AAV1 in ependyma (fig. S2).

A substantial portion of AAVs delivered via the intracerebroventricular route can target peripheral tissues, including the liver (*16*, *17*), with high-dose AAVs inducing toxicity (*18*). Recently, a comprehensive analysis of NHPs infused with CSF-delivered AAVs has shown nonclinical dorsal root ganglion (DRG) pathology in 83% of samples (*15*). DRG toxicity in NHPs has been linked to high transgene expression rather than AAV transduction (*15*, *19*). To examine peripheral, off-target transduction, we performed RNAscope against AAV-derived transcripts in a rhesus macaque injected with 8.8×10^{12} vg of AAV-Ep$^+$.mTFP1 (Fig. 3). We observed little transgene expression in the liver and no detectable transcripts in the heart or DRGs at multiple levels of the spinal cord (Fig. 3, A and B). These data supported AAV-Ep$^+$ for further analysis on the basis of high on-target transgene expression in brain ependyma and neurons with low off-target expression in the periphery.

Delivery of AAV-Ep$^+$ to the posterior lateral ventricles yields superior ependymal transduction

On the basis of the direction of CSF flow through the ventricular system (Fig. 4A), we hypothesized that a posterior site of administration would lead to higher transduction efficiency of ependymal cells in posterior regions of the lateral ventricles with similar transduction efficiency in anterior regions. We tested this hypothesis by delivering 1×10^{13} vg AAV-Ep$^+$.mRuby3 bilaterally into either the anterior or posterior lateral ventricles of four African green monkeys (AGMs), two infused at each anatomical location (Fig. 4A). Qualitatively, posterior infusions yielded more uniform and robust expression throughout the ventricular system (Fig. 4B). As expected, the site of injection did not affect the percentage of transduced ependymal cells in the anterior horn of the lateral ventricles, where transduction percentages averaged 68 and 70% after the anterior (Ant.) and posterior (Post.) infusion, respectively. The site of injection minimally affected transduction of the third ventricle (Ant. 58%, Post. 64%) and the fourth ventricle (Ant. 28%, Post. 44%). In contrast, posterior infusions reproducibly increased the percentage of transduced cells in the lateral ventricle body and in the temporal and posterior regions of the lateral ventricles, with more than 47%

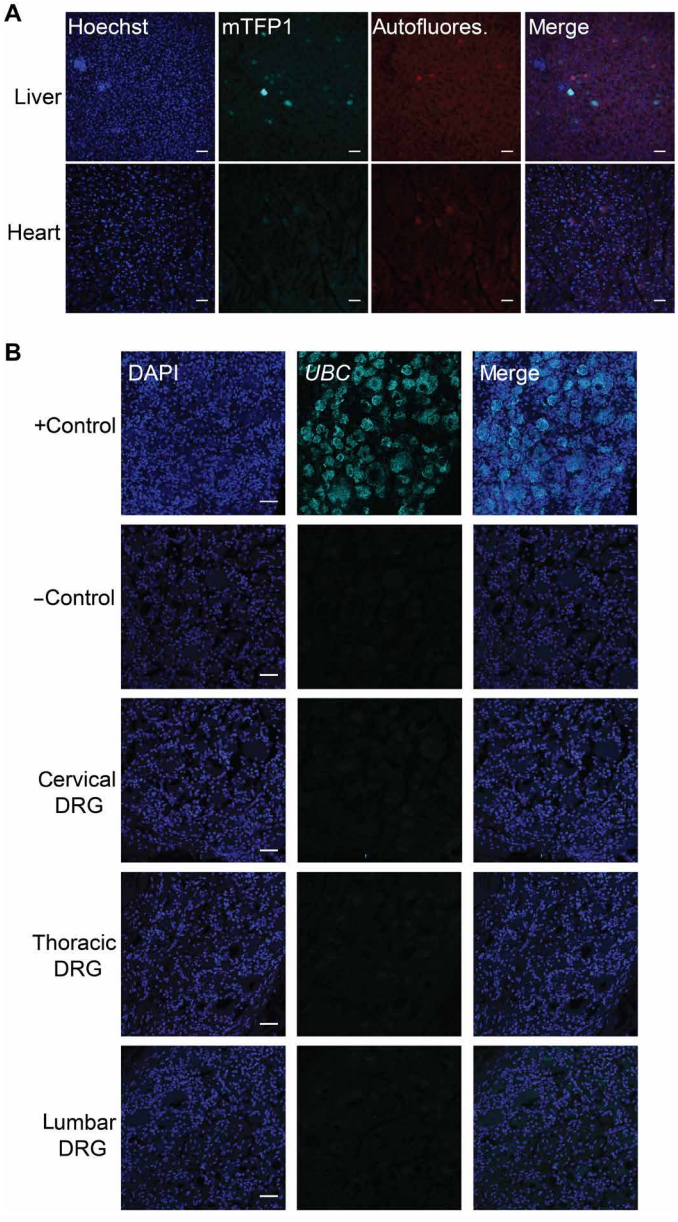

Fig. 3. Low peripheral off-target expression of transgenes delivered by AAV-Ep$^+$ in a rhesus macaque. (**A**) RNA-FISH detection of *mTFP1* transcript in liver and heart. (**B**) RNA-FISH detection of *mTFP1* transcripts in cervical, thoracic, and lumbar DRGs from the same animal examined in (A). *UBC* detection included as a positive assay control. Nuclei are stained blue with DAPI (4′,6-diamidino-2-phenylindole). Scale bars, 50 μm.

of cells transduced and transduction performance over anterior infusion increased by 19- and 11-fold, respectively (Fig. 4C; temporal Ant. 1.09%, Post. 21.35%; posterior Ant. 4.05%, Post. 47.50%). The hippocampus and temporal cortex were also transduced after posterior infusion (Fig. 4D). We infused AAV9.mRuby3 into the posterior lateral ventricle of another animal at the same dose for comparison. At this dose, fewer than 2% of the ependymal cells were transduced with AAV9 (fig. S3). In a separate study with two additional AGMs that received intracerebroventricular injections of 1×10^{13} vg AAV-Ep$^+$.mRuby3, transcripts were present in only 0.3 or 3.3% of numerous sampled DRG neurons at all spinal cord regions (fig. S4). Last, 1×10^{13} vg AAV-Ep$^+$.mRuby3 was infused bilaterally into the posterior lateral ventricle of an adult cynomolgus monkey (Fig. 4E and fig. S5). Transduction of the ependyma was observed throughout the ventricular system (fig. S5, A to C), consistent with results from rhesus macaques and AGMs (Figs. 1 and 2). Together, these data showed robust on-target transduction of ependymal cells after posterior lateral ventricle delivery in NHPs and demonstrated conserved tropism of AAV-Ep$^+$ for ependymal cells across three old world NHP species.

AAV-Ep$^+$ transduces mouse ependyma and human iPSC-derived neurons

Cross-species incompatibility of AAV serotypes can pose challenges to translation of therapeutics from preclinical models to clinical application. In mice, AAV4 delivered to the CSF effectively targets the ependyma but is not efficient in NHPs (*10*, *20*, *21*). In addition, AAV2 transduces ependyma in NHPs and dogs but is not effective in mice (*14*, *17*). To examine cross-species behavior of this NHP-evolved capsid, AAV-Ep$^+$.mRuby3 was infused into the posterior lateral ventricle of adult C57BL/6 and FVB mice ($n = 3$ per strain). Fluorescent reporter expression was evaluated via epifluorescence and was seen in ependyma throughout the ventricular system (Fig. 5A and fig. S6A) and in neurons of the hippocampus and subiculum (Fig. 5B and fig. S6B). Transduced cells were also present in the cortex of both mouse strains (fig. S6, B and C). We also evaluated transduction efficiency of AAV-Ep$^+$ in human neurons derived from iPSCs. At day 40 of differentiation, iPSC-derived cortical neurons were transduced with AAV-Ep$^+$.mRuby3 or its parental serotype AAV1-eGFP at several multiplicities of infection (MOIs; 1×10^3, 1×10^4, and 1×10^5). Ten days after transduction, qualitative analysis by microscopy revealed higher transduction by AAV-Ep$^+$ compared with AAV1 at equivalent doses (Fig. 5C). Quantification by reverse transcription quantitative polymerase chain reaction (RT-qPCR) revealed a 34-fold increase over AAV1 at an MOI of 1×10^3 [Fig. 5D; $P < 0.0001$ for AAV-Ep$^+$ versus AAV1 at 1×10^4 and 1×10^5, respectively; two-way analysis of variance (ANOVA) followed by Bonferroni's correction for multiple comparisons]. These data showed that AAV-Ep$^+$ can transduce cultured human neurons, two strains of mice, and three species of NHPs, further supporting its potential use in preclinical testing for human disease applications.

Intracerebroventricular infusion of AAV-Ep$^+$.hTPP1 delays phenotypes in a mouse model of CLN2 disease and results in therapeutic protein amounts in the CSF of NHPs

Given the observed cross-species compatibility, AAV-Ep$^+$ vectors were tested in a mouse model of CLN2 disease (*22*). AAV-Ep$^+$.hTPP1, with TPP1 expressed from the CAG promoter as before (5×10^{10} vg), or vehicle was infused by intracerebroventricular injection into 7-week-old mice. Five weeks after administration, TPP1 enzyme activity was measured in different brain tissues and compared with that of vehicle-treated *Cln2*$^{+/-}$ and *Cln2*$^{-/-}$ mice. Enzyme activity in *Cln2*$^{-/-}$ mice treated with AAV-Ep$^+$.hTPP1 was 7 to 27 times greater than in heterozygous carriers in superficial and deep regions of the cerebrum as well as the cerebellum (Fig. 6A). The supraphysiological enzyme activity achieved was greater than those achieved after intracerebroventricular delivery of AAV2.caTPP1 at a dose of 1.7×10^{13} vg to CLN2 disease dogs that resulted in marked phenotypic rescue (fig. S7) (*14*). *Cln2*$^{-/-}$ mice have a survival deficit

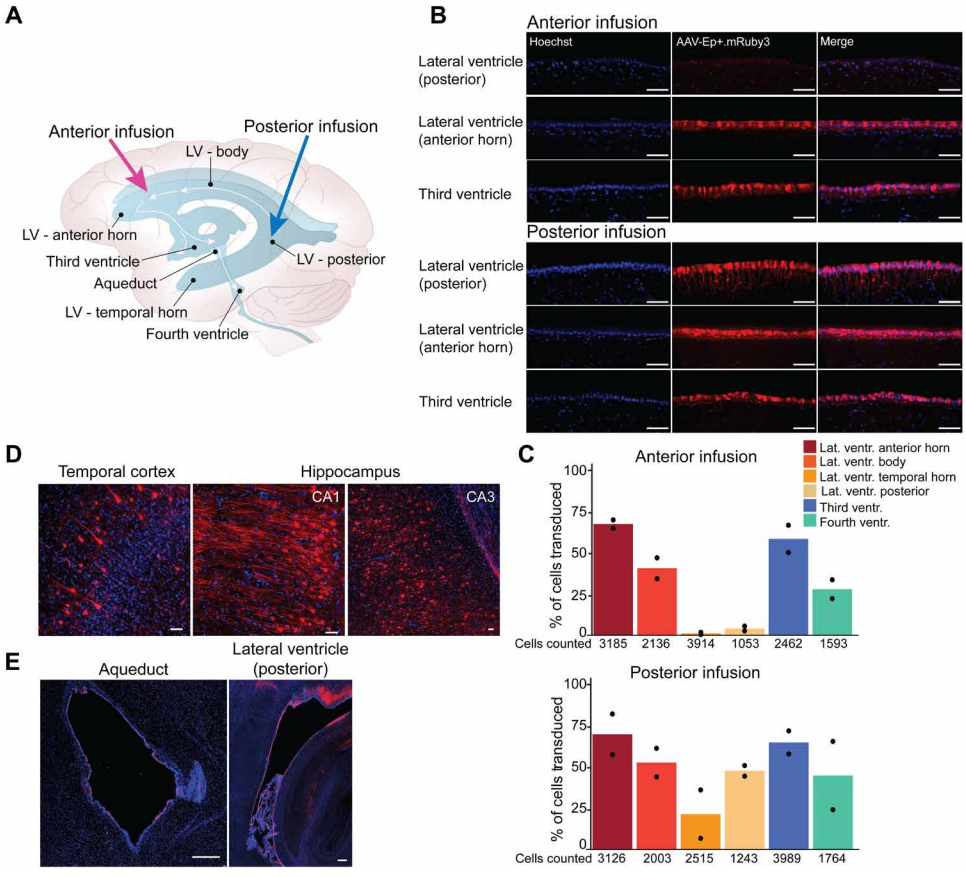

Fig. 4. Posterior lateral ventricle infusion of AAV-Ep$^+$ improves ependymal transduction over anterior infusion in African green monkeys. (**A**) Depiction of the NHP ventricular system. Arrows indicate anterior (magenta) and posterior (blue) injection sites. (**B**) Representative high-magnification images of Hoechst (left) and mRuby3 (right) fluorescence of AGM ependyma in two locations in the lateral ventricles and the third ventricle 4 weeks after delivery of AAV-Ep$^+$.mRuby3 at anterior (top) or posterior (bottom) coordinates. (**C**) Quantification of ependymal cell transduction at indicated locations. Dots indicate individual animals. (**D**) Representative images of mRuby3 fluorescence in parenchymal areas 4 weeks after posterior intracerebroventricular delivery. (**E**) Representative images of mRuby3 fluorescence in cynomolgus monkey ependyma 4 weeks after infusion of AAV-Ep$^+$.mRuby3 in the posterior lateral ventricle. Scale bars, 50 μm [(B) to (D)] and 500 μm (E).

and a tremor phenotype that emerges at 12 weeks and is quantifiable at 24 and 52 Hz (*6*). To assess the effects of AAV-Ep$^+$.hTPP1 on these phenotypes, a second cohort of CLN2 mice was intracerebroventricularly injected as above at 7 weeks of age for survival and tremor analysis. Comparison of tremor in control and treated mice revealed significant improvements with AAV-Ep$^+$.hTPP1 treatment at specific frequencies by 12 weeks of age that reached significance by area under the curve for the total spectrum by 16 weeks of age (Fig. 6B, $P < 0.05$ by two-way ANOVA mixed-effect model followed by Bonferroni multiple comparisons post hoc test). In addition, life span was modestly but significantly extended relative to vehicle-treated controls (Fig. 6C; $P < 0.05$ by log rank Mantel-Cox test).

To further assess the translatability of this approach, 1×10^{12} vg of AAV-Ep$^+$.hTPP1 or vehicle was infused bilaterally into the posterior lateral ventricle of two cynomolgus monkeys. CSF was obtained before injection (baseline) and again at 7, 14, and 28 days postinfusion. CSF TPP1 concentrations were measured using a capillary Western blot system with an antibody that cross-reacts with human and NHP TPP1. Animals showed a time-dependent increase in TPP1 proenzyme concentrations, reaching three times and six times that of baseline at 28 days (Fig. 6D). The concentration of human TPP1 produced minus the cynomolgus monkey baseline was 5 and 9 times higher than that found in the CSF from children without CLN2 disease (Fig. 6E). In contrast, earlier work reported that intracisterna magna infusion of 5×10^{13} vg AAVrh10 into NHPs achieved only 43 to 62% of normal human TPP1 concentrations in the CSF on average (*23*). Together, these mouse and NHP studies of AAV-Ep$^+$.hTPP1 support its further development for potential clinical application.

DISCUSSION

Our previous work showed that intracerebroventricular delivery of ependyma-specific AAV capsids enables broad distribution of lysosomal enzymes for therapeutic benefit in mouse and dog models of LSDs (*10*, *14*). In this study, we identified AAV capsid variants enriched for transduction of NHP ependyma and brain parenchyma and showed that the lead candidate, AAV-Ep$^+$, could improve survival and tremor in a mouse model of CLN2 disease. Further, intracerebroventricular delivery of AAV-Ep$^+$.TPP1 to NHPs resulted in similar or greater concentrations of proTPP1 in the CSF as observed after intracisterna magna delivery of AAV.rh10 (*13*) with 50× less virus or AAV9 (*19*) with 30× less virus.

We chose to screen capsids in NHPs on the basis of previous work showing that selection strategies in murine model systems do not translate to larger mammals (*24*, *25*). Our initial screening library was composed of variants derived from three different parental serotypes (AAV1, AAV2, and AAV9), all known to transduce the brain. Our top variant was derived from AAV1 rather than the more commonly used AAV9, highlighting the value of including multiple serotypes in capsid-discovery efforts. Similar to our other capsid enrichment campaign (*26*), our NHP-derived top candidate (AAV-Ep$^+$) achieved high on-target and low off-target transduction. AAV-Ep$^+$ transduced large portions of cells lining the ventricles

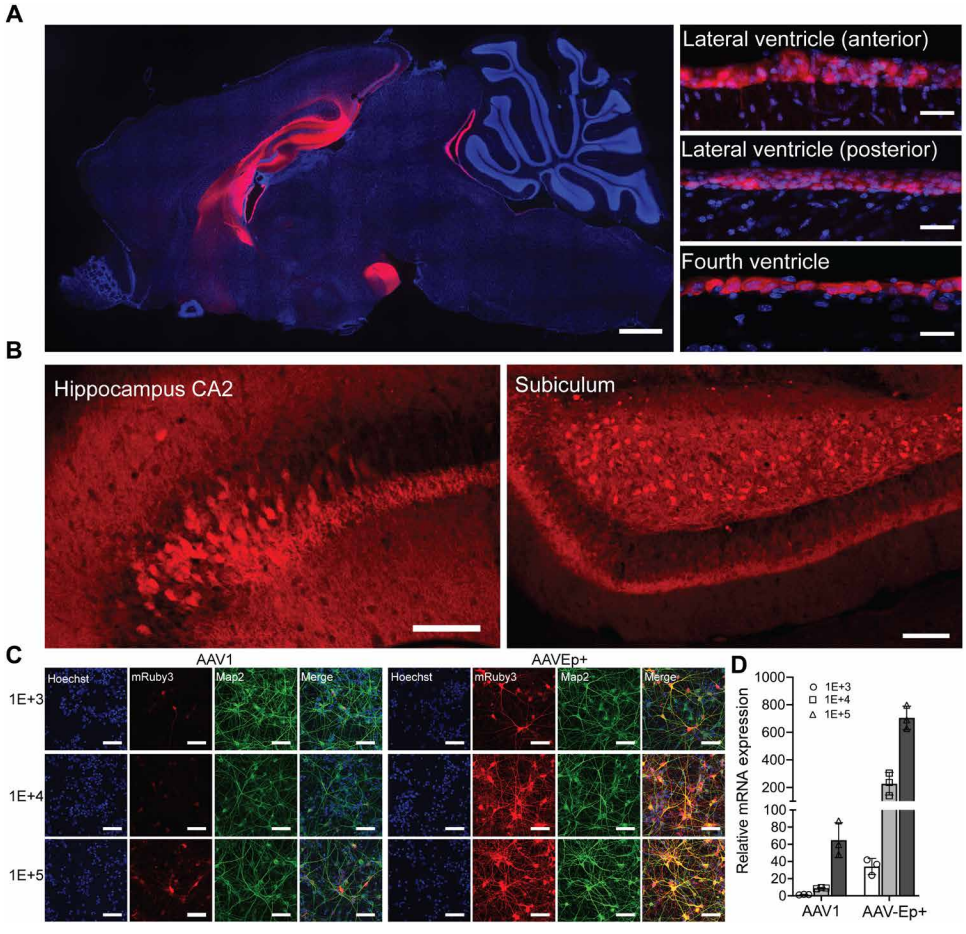

Fig. 5. AAV-Ep$^+$ transduces mouse brain ependyma and parenchyma and human iPSC-derived cortical neurons. (**A**) Representative tile scan and high-magnification images demonstrating Hoechst (blue) and mRuby3 (red) fluorescence in the brain of an adult FVB mouse infused 4 weeks earlier with AAV-Ep$^+$.mRuby3 at 1×10^{10} vg. Similar transduction profiles were observed in three animals. Scale bars, 1 mm or 100 μm (zoom). (**B**) Representative images of the hippocampus (left) and subiculum (right) demonstrating mRuby3 fluorescence in neurons. Scale bars, 100 μm. (**C**) Representative Hoechst (blue), mRuby3 (red), or MAP2 (green) fluorescence in human iPSC-derived cortical neurons 10 days after transduction with AAV-Ep$^+$.mRuby3 or AAV1.mRuby3 at indicated MOIs. Scale bars, 50 μm. (**D**) Transgene expression quantified by RT-qPCR. All samples were normalized to *GAPDH* and are presented relative to AAV1.eGFP at a dose of 1×10^3. Each dot represents a biological replicate. $P < 0.0001$ for AAV-Ep$^+$ versus AAV1 at 1×10^4 and 1×10^5, respectively; two-way ANOVA with Bonferroni's correction.

with greater than 20-fold higher potency than its parental serotype, AAV1 (fig. S2), and with even higher efficiency relative to AAV9. The high transduction efficiency in mice, multiple NHP species, and human iPSC neurons highlights AAV-Ep$^+$ as a serious candidate for clinical translation.

Another feature of our screen was our choice of the intracerebroventricular route of administration to better expose vector to the largely postmitotic ependymal cells (*27*, *28*) and brain parenchyma for secretion of therapeutic molecules into the CSF. We found that the location of infusion affects transduction efficiency, with increased transduction being achieved when the direction of CSF flow was considered. It is presumably due to the direction of CSF flow that AAVs delivered via the cisterna magna do not efficiently transduce brain (*29*).

Potential applications for AAV-Ep$^+$ include treatment of genetic diseases caused by loss of enzyme function, including LSDs wherein the deficient enzyme is a soluble lysosomal hydrolase, such as TPP1 as shown here. AAV-based therapies applied thus far for CLN2 disease use direct parenchymal injection of AAV2 or AAVrh.10, with more recent efforts delivering AAVrh.10 via intracisterna magna injection (*23*, *30*). AAV-Ep$^+$–based gene therapies would be delivered via intracerebroventricular injection, a well-established method for delivering therapeutics to the central nervous system that results in broad brain distribution (*31*). In previous work, we treated TPP1-deficient dogs with 1.7×10^{13} vg of AAV2.caTPP1, which resulted in normalized enzyme activity in the brain, markedly extended life spans, and improved motor skills and social interactions (*14*). Unlike AAV2, AAV-Ep$^+$ transduced brain parenchyma and ependyma and may provide greater therapeutic benefit with a similar approach and at lower doses.

This study does have some limitations. First, although AAV-Ep showed broad transduction across NHP species, mice strains, and in human neurons derived from iPSCs, the ability of AAV-Ep$^+$ to transduce human brain remains unknown. Further studies testing AAV-Ep$^+$ on brain organoids will be informative in this regard. However, only by testing in clinical trials will the true translational utility of AAV-Ep$^+$, or any capsid evolved for brain delivery, be known. Second, the mouse and NHP studies with AAV-Ep$^+$.hTPP1 expressed a human protein in animal models without immunosuppression, and immune response to the transgene may confound results. Immunosuppression in the *Cln2*$^{-/-}$ mice may result in even greater effects on tremor and survival after treatment with AAV-Ep$^+$.hTPP1.

We predict that the lower vector genome doses permitted by AAV-Ep$^+$ may lead to an improved safety profile and larger therapeutic index than conventional AAV gene therapies. Beyond the treatment of LSDs, AAV-Ep$^+$ may also be suitable for expression of nanobodies or other small, secreted antibody fragments to target extracellular proteins or intracellular disease targets or to increase their effect via cross-correction from transduced cells in the brain (*32*–*34*). It may also be well suited for broad distribution of secreted growth factors as a treatment for Parkinson's disease or amyotrophic

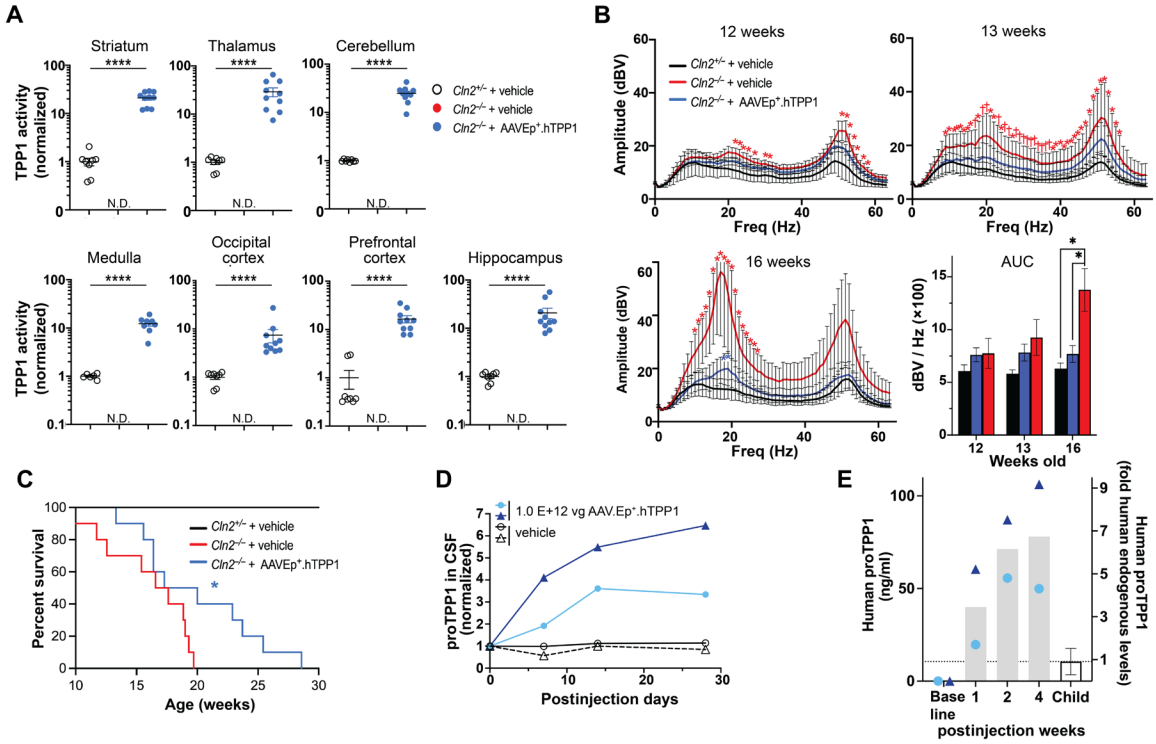

Fig. 6. Functional correction of *Cln2*$^{-/-}$ mice and hTPP1 expression in NHPs with AAV-Ep^{+}.hTPP1 treatment. (**A**) TPP1 enzymatic activity in tissue lysates from mice infused with 5×10^{10} vg AAV-Ep^{+} at 7 weeks of age and harvested 5 weeks later (*Cnl2*$^{-/-}$ + AAV-Ep^{+}.hTPP1, $n = 10$; *Cln2*$^{-/-}$, $n = 6$; *Cln2*$^{+/-}$, $n = 8$). No enzymatic activity was observed in vehicle-treated *Cln2*$^{-/-}$ mice (N.D., not detected). ****$P < 0.0005$, by two-tailed Mann-Whitney *U* test. (**B**) Resting tremor amplitude at the indicated frequencies during a 5-min recording interval (*Cln2*$^{-/-}$ + AAV-Ep^{+}.hTPP1, $n = 10$; *Cln2*$^{-/-}$, $n = 7$; *Cln2*$^{+/-}$, $n = 9$ at 12 weeks; *Cln2*$^{-/-}$ + AAV-Ep^{+}.hTPP1, $n = 8$; *Cln2*$^{-/-}$, $n = 7$; *Cln2*$^{+/-}$, $n = 9$ at 13 weeks; and *Cln2*$^{-/-}$ + AAV-Ep^{+}.hTPP1, $n = 6$; *Cln2*$^{-/-}$, $n = 5$; *Cln2*$^{+/-}$, $n = 9$ at 16 weeks). Lower right graph in (B) represents area under the curve of whole resting tremor amplitude spectrum (0 to 63 Hz) over time for each treatment group that was analyzed [*$P < 0.05$, †$P < 0.01$ by two-way ANOVA (mixed-effect model) followed by Bonferroni multiple comparisons post hoc test]. (**C**) Survival curves for mice treated with 5×10^{10} vg AAV-Ep^{+}.hTPP1 at 7 weeks of age (*Cln2*$^{-/-}$ + AAV-Ep^{+}.hTPP1, $n = 10$; *Cln2*$^{-/-}$, $n = 10$; *Cln2*$^{+/-}$, $n = 9$, *$P < 0.05$ by log rank Mantel-Cox test). (**D**) Pro-TPP1 protein abundance in CSF normalized to each animal's baseline values from 1, 2, and 4 weeks after intracerebroventricular injection of AAV-Ep^{+}.hTPP1 into cynomolgus monkeys (5×10^{11} vg AAV-Ep^{+}.hTPP1/hemisphere, 1×10^{12} vg total). (**E**) Human TPP concentrations (ng/ml) in CSF expressed from AAV-Ep^{+}.hTPP1–treated NHP compared with endogenous TPP1 in nine human CSF samples. All data are expressed as mean ± SEM.

lateral sclerosis (*35*). In conclusion, using AAV capsid screens in NHPs, we identified AAV-Ep^{+} as a potent vector for gene therapy applications where CSF protein expression is required.

MATERIALS AND METHODS

Study design

The overall objectives of the study were to identify AAV capsid variants with brain tropism after intracerebroventricular injection in NHPs and to assess the translational potential of a top AAV capsid variant in NHPs, mice, and human iPSC-derived neurons. NHP experiments included one or two animals per group, and wild-type mouse experiments included three animals per group. Experimenters were not blinded to treatment group for NHP and wild-type mouse experiments. Human iPSC experiments were conducted with three biological replicates of three or four technical replicates. *Cln2*$^{-/-}$ mouse experiments included 7 to 10 animals per group. Experimenters were blinded to treatment group while conducting the tremor assay. All animal experiments were conducted in accordance with the *Guide for the Care and Use of Laboratory Animals* (National Research Council), and mouse and NHP procedures were approved by the Children's Hospital of Philadelphia (CHOP) Research Institutional Animal Care and Use Committee (protocol numbers 23-001358 and 25-001328, respectively).

Peptide-modified AAV library description and construction

Library plasmids were constructed by cloning the AAV2 Rep open reading frame and AAV Cap open reading frames of different serotypes into an AAV2-inverted terminal repeat–containing plasmid. Silent sequence modifications were made in the Cap coding sequence to introduce restriction enzyme (RE) sites around the peptide insertion site. Oligonucleotides encoding the random 7-mer $(NNK)_7$ were synthesized by Integrated DNA Technologies and cloned into the RE-digested recipient plasmids using Gibson Assembly. Pooled plasmids were transformed into Endura electrocompetent cells (LGC), and plasmid isolation was performed using Qiagen Giga Prep Endofree kits (QIAGEN). For the second round of library generation, viral genomic DNA from collected tissues was isolated by QIAamp DNA mini kits (QIAGEN), and the variable region of the AAV library was amplified using serotype-specific primers. Amplicons were incorporated into recipient plasmids by Gibson Assembly and transformed into Endura electrocompetent cells (LGC).

Pooled, purified variant plasmids were used to generate the round two library.

AAV production

AAVs were generated by the CHOP Research Vector Core. For AAV library production, human embryonic kidney 293 cells from ATCC (the American Type Culture Collection) were transfected with pAd helper and pAAV.Lib plasmids, the latter at an average of 1000 plasmid copies per cell to reduce cross-packaging. Recombinant virus was harvested and purified by two rounds of cesium chloride gradient centrifugation. Plasmids encoding the capsids selected for further evaluation were used in the final studies, each encoding a different fluorophore as noted in the figure legends. In all cases, the sequences were cloned into the AAV Cap gene in loop 8 of viral protein VP3 along with flanking Gly/Ser amino acids. Insertions were made at amino acid positions 590, 587, and 588 for AAV1, AAV2 and AAV9, respectively.

Gene blocks of hTPP1 cDNA and multiple fluorescent reporters (mTFP1, mRuby3, mNeonGreen, and mTagBFP) were purchased from IDT (Integrated DNA Technologies) and cloned into an AAV backbone plasmid with CAG promoter and BGHpA. AAVs were titered by droplet digital PCR with ITR primer probe for AAV library vectors, CAG promoter primer probe for fluorescent vector, and hTPP1 primer probe for hTPP1 vectors. Sequences of primer probes are listed in table S2.

NHP procedures

NHPs were housed at the CHOP Research Institute under a 12-hour light:dark cycle with ad libitum access to purified drinking water and twice daily feedings with Purina LabDiet certified primate diet (5048) enriched with fruits and vegetables.

NHPs were injected with test articles or vehicle control as indicated in table S1. AAV formulation buffer was used as vehicle control and to dilute viruses to the desired titer for injection. Before all intracerebroventricular injections, animals were sedated with either ketamine and xylazine or Telazol followed by isoflurane anesthesia for the duration of the procedure. For stereotaxic intracerebroventricular injections, baseline MRI scans were used to define trajectories. Cannula placement was confirmed by fluoroscopy using IsoVue M contrast before infusing test article. For ClearPoint intracerebroventricular injections, the animal was sedated as above and positioned in the MRI scanner, and the ClearPoint system was used to define target coordinates and calculate cannula tracks. The test article was mixed with ProHance gadolinium contrast (1.8 mM final concentration) to visualize the infusate and confirm cannula placement. After a 10-min dwell period, the cannula was removed, the skin was sutured, and the animal recovered. Buprenorphine sustained release was given as analgesia, and the animals were monitored postoperatively for pain and welfare.

NHPs were euthanized by exsanguination. Animals were sedated, transcardially perfused with ice-cold saline, and the brain was removed and processed into 4-mm coronal slabs in a rhesus macaque or cynomolgus brain matrix, respectively. For AAV library experiments, tissue samples from ependyma, cerebral cortex, hippocampus, caudate, putamen, thalamus, pons, and cerebellar cortex were microdissected and flash frozen for recovery of AAV amplicons for the next round of evaluation.

NHP fluorescence validation

For fluorescence microscopy analyses, animals were euthanized by transcardial perfusion with ice-cold saline after sedation, and the brains were removed and slabbed into 4-mm coronal slabs. Brain slabs, DRGs, and other tissues were postfixed in 4% paraformaldehyde, cryoprotected by sequential immersion in 15 and 30% sucrose in 0.1 M phosphate-buffered saline (PBS) baths for 2 days each step at 4°C. Forty-millimeter-thick sections were prepared with a Leica SM2010R microtome attached to a BSF-30MP freezing stage (Physitemp). Sections were rinsed in 0.1 M PBS and incubated in 1/5000 Hoechst for 1 min before being mounted in superfrost plus slides. Coverslips were mounted with Fluoromount-G (SouthernBiotech, #0100-01). Slides were analyzed with a Leica DM6000B epifluorescence microscope equipped with a Hammatsu ORCAFlash 4.0 monochrome camera and Leica LED 405, L5 ET, Y3 ET, TXT ET, Chroma 39001 AT-ECFP/C, and 49003 ET-EYFP filter cubes.

Amplicon sequencing of AAV libraries

Genomic DNA (gDNA) or RNA from harvested tissues (ependyma plus cortical, subcortical, and cerebellar regions) was isolated using a QIAamp DNA mini kit or RNeasy Plus kit (QIAGEN). Variant amplicon libraries were generated using two rounds of PCR. In the first round, sequence encoding the modified capsid insertion was amplified using serotype-specific primers with PCR cycles less than 30 using the Q5 2× master mix (New England Biolabs). First-round PCR products were used as input for the second PCR that introduced Illumina i5 and i7 sequencing indices and adapters. Sizes of second-round amplicon DNA were checked by agarose gel and purified using a MinElute gel extraction kit (QIAGEN). For all libraries, sequencing was done on an Illumina NovaSeq 6000 using a 200-cycle reagent kit and paired-end read chemistry yielding 100–base pair paired-end read outputs. Initial quality control of Illumina FASTQs was performed by testing for perfect string matches to known constant regions of the amplicons. Capsid variant identity and abundance were quantified from passing reads by tabulating the occurrence of unique nucleic acid sequences encoding the heptamer peptide inserts. Variant abundance was quantified as the unique molecular identifier (UMI) collapsed read count for each unique sequence. A baseline variant performance threshold was applied by removing any variants with UMI counts <100. In addition, potential sequencing errors were removed by filtering out variants that had <1% of the UMI counts and were within one edit distance of another variant. Capsid variant performance within each tissue was assessed using two primary metrics: variant abundance (UMI counts) and an enrichment score. The enrichment score measures the fold change in a capsid variant's abundance in a tissue compared with its abundance in the injected virus library (input virus)

$$\mathrm{UMIpct}_{x,\mathrm{tissue}} = \frac{\mathrm{UMI}_{x,\mathrm{tissue}}}{\sum_{i=1}^{N_{\mathrm{tissue}}} \mathrm{UMI}_{i,\mathrm{tissue}}} \quad (1)$$

$$\mathrm{UMIpct}_{x,\mathrm{inputvirus}} = \frac{\mathrm{UMI}_{x,\mathrm{inputvirus}}}{\sum_{i=1}^{N_{\mathrm{tissue}}} \mathrm{UMI}_{i,\mathrm{inputvirus}}} \quad (2)$$

$$\text{Enrichment}_x = \left(\frac{\text{UMIpct}_{x,\text{tissue}} - \text{UMIpct}_{x,\text{inputvirus}}}{\text{UMIpct}_{x,\text{inputvirus}}} \right) + 1 \quad (3)$$

Capsid variant performance was assessed using DNA and RNA data, UMI counts and enrichment metrics, and single-region (targeted) and cross-region analyses. Selection of capsids for validation was done after considering the totality of available data. No single data/metric/region combination served as a singular deciding factor.

RNAscope-FISH

Four-millimeter coronal slabs postfixed in 4% paraformaldehyde brain slabs were sucrose cryoprotected, cut in 2 cm–by–2 cm blocks, and embedded in optimal cutting temperature compound. Slices (16 μm thick) were collected on Superfrost Plus slides after microtomy with a Leica CM1950 cryostat. Fluorescence in situ hybridization (FISH) was performed using an RNAscope multiplex fluorescent reagent kit v2 assay (Advanced Cell Diagnostics, cat. no. 323100-USM) following the manufacturer's guidelines. *mTFP1* and *mRuby3* RNAscope probes (Advanced Cell Diagnostics cat. nos. 500271-C3 and 557101-C4) were used to detect fluorophore transcripts in the DRGs. Opal620 and Opal690 fluorophores (Akoya Biosciences, FP1495001KT and FP1497001KT) were associated to the mTFP1-C3 and mRuby3-C4 probes, respectively. Slides were observed under a Leica SP8 confocal microscope.

Mouse biodistribution studies

Mice were maintained on a 12-hour light/dark cycle and ad libitum access to water and food. Adult C57BL/6 and FVB mice ($n = 3$, JAX strains #000664 and #01800) were injected with AAV-Ep$^+$.mRuby3 at 1×10^{10} vg. Injections targeting lateral ventricle (from bregma in millimeters: AP, −2.18; ML, ±2.9; DV, 3.5) were done at a rate of 25 nl/min. Three weeks after injection, mice were transcardially perfused with 0.05 M PBS, pH 7.4, followed by 50 ml of 4% w/v paraformaldehyde in phosphate buffer (0.1 M, pH 7.4). Brains were cryoprotected and sectioned in the sagittal plane. For each brain, the sites of injection were verified, and sections were analyzed using a Leica DM6000B epifluorescence microscope for low-power and tiled images. Z-stacks were acquired using a Leica SP8 confocal microscope. Both microscopes were under the control of Leica LAS X v3.7 software.

Automated cell counting

Automated cell counting was used to evaluate transduction in confocal images from AAV-Ep$^+$–treated (348 images) and AAV9-treated (230 images) NHPs (QuPath v0.4.4) (*36*). For quantitation of AAV-Ep$^+$ transduction, 30,006 total ependymal cells were defined and counted as either AAV-Ep$^+$.mRuby3 positive or negative using a centroid-based fluorescence intensity threshold. For quantitation of AAV9 transduction, 22,458 total ependymal cells were defined and counted as either AAV9.mRuby3 positive or negative. Nuclei within the region of interest were defined by Hoechst signal. Because no cytoplasmic marker was available, a small uniform cytoplasmic expansion was created around each defined nucleus. A threshold-based cell classifier was applied to define the positive/negative status of each cell. Aggregated cell counts from each image were exported and processed using a custom R pipeline for data analysis and visualization.

Human iPSC-derived neuron transduction

iPSC-derived cortical excitatory neurons were generated from iPSCs as previously described (*37*). After 40 days of differentiation, cells were transduced with differing MOIs based on initial cell plating counts. Ten days later, RNA was isolated for qRT-PCR using a Quick-RNA miniprep kit according to the manufacturer's instructions (Zymo Research). For microscopy, iPSC-derived cortical neurons were seeded on coverslips and transduced as above. At 10 days posttransduction, cells were fixed and blocked, and fluorescence was assessed using epifluorescent microscopy (Leica, DM6000B).

Cln2$^{-/-}$ mice

Cln2$^{-/-}$ mice have been described previously (*22*) and were obtained from P. Lobel, Rutgers University, then backcrossed to C57BL/6J mice at the CHOP Research Institute. This mouse model has a neo cassette insertion between exons 11 and 12 that, in homozygosity, results in no detectable TPP1 activity. *Cln2*$^{-/-}$ mice or heterozygous littermates were injected into the lateral ventricle with either 5×10^{10} vg of AAV-Ep$^+$.hTPP1 or vehicle control (AAV formulation buffer) at 7 weeks of age. Animals were anesthetized with isoflurane, and the surgical depth of anesthesia was confirmed by toe/tail pinch and eyeblink reflex. The injection coordinates were 0.3 mm anterior, 1 mm lateral, and 2 mm depth, and a 10-μl volume was injected into the right ventricle at a 0.33-μl/min infusion rate. After injection, the subject was allowed to recover in a warming chamber until a normal range of activity was regained. Mice were then returned to the home cage.

TPP1 activity assay

Five weeks after injection, mice were anesthetized with isoflurane and transcardially perfused with 10 ml of ice-cold 0.1 M PBS, pH 7.4. Brains were harvested and microdissected. Samples were then stored at −80°C until processing. Thawed tissues were homogenized in ice-cold homogenization buffer (0.1% Triton X-100 in 0.1 M PBS), with complete protease inhibitor cocktail (Roche). Insoluble material was removed from the homogenate by centrifugation at 21,000*g* at 4°C for 15 min, and protein content in the supernatant was quantified by DC protein assay (Bio-Rad). Homogenate (10 μl) was added to wells of a 96-well black wall/clear bottom plate containing 80 μl of sodium citrate buffer (pH 4.0). The enzyme reaction was initiated by the addition of 10 μl of substrate (250 μM Ala-Ala-Phe 7-amido-4 methylcoumarin in sodium citrate buffer, pH 4.0) and read every 3 min for 2 hours in a SpectraMax M5 microplate reader (Molecular Devices) at 37°C with a 460-nm emission filter. TPP1 activity was calculated as the change in fluorescence units (FU) per minute. Absolute quantification was calculated using an hTPP1 standard curve (Novus Biologicals, 2237-SE-010) preactivated in sodium citrate buffer for 12 hours at room temperature.

Tremor activity monitoring and survival

Tremor activity was quantified with a San Diego Instruments tremor monitor (SDI). Animals were acclimated in the behavior room for 30 min before the experiment. Once inside the apparatus, the mouse was allowed to habituate in the animal enclosure for 3 min before recording tremor activity for 5 min. Tabulation of tremor activities was analyzed by SDI data software. Mice were randomly assigned to experimental groups using the RAND function in Excel (Microsoft) after genotyping. The *Cln2*$^{+/-}$ plus vehicle group consisted of nine (five females and four males) mice, the *Cln2*$^{-/-}$ plus vehicle

group had 10 (5 females and 5 males) mice, and the *Cln2*$^{-/-}$ plus AAV-Ep^{+}.hTPP1 was composed of 10 (5 females and 5 males) mice.

hTPP1 proenzyme quantification

TPP1 proenzyme in CSF were quantified using a capillary Jess Simple Western blot system (Protein Simple, Bio-Techne) and Compass software (Protein Simple) following the manufacturer's indications. Absolute quantitation was calculated from a six-point standard curve (0.03 to 1 ng/ml) generated with human recombinant TPP1 (Novus Biologicals, 2237-SE-010) diluted with 0.1× sample buffer (Protein Simple, no. 042-195). CSF and standard curve samples were combined with 5× fluorescent master mix at a 4:1 ratio, denatured at 95°C for 5 min, spun down at 4°C, and then loaded into a 12- to 230-kDa separation capillary cartridge (Protein Simple, no. SM-W004). A ratio of 1:50 mouse anti-TPP1 monoclonal antibody (Abcam, ab54685) and anti-mouse detection module (Protein Simple, no. DM-002) was used for TPP1 detection. Note that this anti-TPP1 antibody does not distinguish human and cynomolgus monkey TPP1. Therefore, human TPP1 protein concentration was estimated by subtracting each animal's baseline TPP1 CSF concentration from the total CSF concentrations at the measurement timepoints.

Statistical analysis

GraphPad Prism 10 software (GraphPad Software) and G*Power 3.1.9.6 (Heinrich Heine Universität, Düsseldorf, Germany) software packages were used for statistical analyses. None of the groups analyzed for TPP1 activity in the mouse experiment (Fig. 6A) passed the Anderson-Darling normality test. Statistical significance was assessed by the two-tailed Mann-Whitney test. Resting tremor was analyzed by unbalanced mixed-effects analysis followed by a Dunnett's multiple comparation test. Resting tremor plots showing amplitude for the frequency range are expressed as mean ± SD by two-way ANOVA (mixed-effect model) followed by the Bonferroni multiple comparisons post hoc test. Survival was analyzed by the log-rank Mantel-Cox test.

Supplementary Materials

The PDF file includes:
Figs. S1 to S7
Tables S1 and S2
Legend for data file S1

Other Supplementary Material for this manuscript includes the following:
Data file S1
MDAR Reproducibility Checklist

REFERENCES AND NOTES

1. F. M. Platt, A. d'Azzo, B. L. Davidson, E. F. Neufeld, C. J. Tifft, Lysosomal storage diseases. *Nat. Rev. Dis. Primers.* **4**, 27 (2018).
2. C. Fernandez-Pereira, B. San Millan-Tejado, M. Gallardo-Gomez, T. Perez-Marquez, M. Alves-Villar, C. Melcon-Crespo, J. Fernandez-Martin, S. Ortolano, Therapeutic approaches in lysosomal storage diseases. *Biomolecules* **11**, 1775 (2021).
3. R. J. Ziegler, E. A. Salegio, J. C. Dodge, J. Bringas, C. M. Treleaven, S. D. Bercury, T. J. Tamsett, L. Shihabuddin, P. Hadaczek, M. Fiandaca, K. Bankiewicz, R. K. Scheule, Distribution of acid sphingomyelinase in rodent and non-human primate brain after intracerebroventricular infusion. *Exp. Neurol.* **231**, 261–271 (2011).
4. R. W. Barton, E. F. Neufeld, The Hurler corrective factor. Purification and some properties. *J. Biol. Chem.* **246**, 7773–7779 (1971).
5. M. S. Sands, B. L. Davidson, Gene therapy for lysosomal storage diseases. *Mol. Ther.* **13**, 839–849 (2006).
6. M. Chang, J. D. Cooper, D. E. Sleat, S. H. Cheng, J. C. Dodge, M. A. Passini, P. Lobel, B. L. Davidson, Intraventricular enzyme replacement improves disease phenotypes in a mouse model of late infantile neuronal ceroid lipofuscinosis. *Mol. Ther.* **16**, 649–656 (2008).
7. M. A. Passini, J. C. Dodge, J. Bu, W. Yang, Q. Zhao, D. Sondhi, N. R. Hackett, S. M. Kaminsky, Q. Mao, L. S. Shihabuddin, S. H. Cheng, D. E. Sleat, G. R. Stewart, B. L. Davidson, P. Lobel, R. G. Crystal, Intracranial delivery of CLN2 reduces brain pathology in a mouse model of classical late infantile neuronal ceroid lipofuscinosis. *J. Neurosci.* **26**, 1334–1342 (2006).
8. T. Ichimura, P. A. Fraser, H. F. Cserr, Distribution of extracellular tracers in perivascular spaces of the rat brain. *Brain Res.* **545**, 103–113 (1991).
9. D. J. Wolak, R. G. Thorne, Diffusion of macromolecules in the brain: Implications for drug delivery. *Mol. Pharm.* **10**, 1492–1504 (2013).
10. G. Liu, I. Martins, J. A. Wemmie, J. A. Chiorini, B. L. Davidson, Functional correction of CNS phenotypes in a lysosomal storage disease model using adeno-associated virus type 4 vectors. *J. Neurosci.* **25**, 9321–9327 (2005).
11. D. E. Sleat, R. J. Donnelly, H. Lackland, C. G. Liu, I. Sohar, R. K. Pullarkat, P. Lobel, Association of mutations in a lysosomal protein with classical late-infantile neuronal ceroid lipofuscinosis. *Science* **277**, 1802–1805 (1997).
12. I. Sohar, D. E. Sleat, M. Jadot, P. Lobel, Biochemical characterization of a lysosomal protease deficient in classical late infantile neuronal ceroid lipofuscinosis (LINCL) and development of an enzyme-based assay for diagnosis and exclusion of LINCL in human specimens and animal models. *J. Neurochem.* **73**, 700–711 (1999).
13. D. Sondhi, D. A. Peterson, E. L. Giannaris, C. T. Sanders, B. S. Mendez, B. De, A. B. Rostkowski, B. Blanchard, K. Bjugstad, J. R. Sladek Jr., D. E. Redmond Jr., P. L. Leopold, S. M. Kaminsky, N. R. Hackett, R. G. Crystal, AAV2-mediated CLN2 gene transfer to rodent and non-human primate brain results in long-term TPP-I expression compatible with therapy for LINCL. *Gene Ther.* **12**, 1618–1632 (2005).
14. M. L. Katz, L. Tecedor, Y. Chen, B. G. Williamson, E. Lysenko, F. A. Wininger, W. M. Young, G. C. Johnson, R. E. Whiting, J. R. Coates, B. L. Davidson, AAV gene transfer delays disease onset in a TPP1-deficient canine model of the late infantile form of Batten disease. *Sci. Transl. Med.* **7**, 313ra180 (2015).
15. J. Hordeaux, E. L. Buza, C. Dyer, T. Goode, T. W. Mitchell, L. Richman, N. Denton, C. Hinderer, N. Katz, R. Schmid, R. Miller, G. R. Choudhury, M. Horiuchi, K. Nambiar, H. Yan, M. Li, J. M. Wilson, Adeno-associated virus-induced dorsal root ganglion pathology. *Hum. Gene Ther.* **31**, 808–818 (2020).
16. E. K. Meseck, G. Guibinga, S. Wang, C. McElroy, E. Hudry, K. Mansfield, Intrathecal sc-AAV9-CB-GFP: Systemic distribution predominates following single-dose administration in cynomolgus macaques. *Toxicol. Pathol.* **50**, 415–431 (2022).
17. D. J. Ballon, J. B. Rosenberg, E. K. Fung, A. Nikolopoulou, P. Kothari, B. P. De, B. He, A. Chen, L. A. Heier, D. Sondhi, S. M. Kaminsky, P. D. Mozley, J. W. Babich, R. G. Crystal, Quantitative whole-body imaging of I-124-labeled adeno-associated viral vector biodistribution in nonhuman primates. *Hum. Gene Ther.* **31**, 1237–1259 (2020).
18. E. Hudry, F. Aihara, E. Meseck, K. Mansfield, C. McElroy, D. Chand, F. F. Tukov, K. Penraat, Liver injury in cynomolgus monkeys following intravenous and intrathecal scAAV9 gene therapy delivery. *Mol. Ther.* **31**, 2999–3014 (2023).
19. N. Buss, L. Lanigan, J. Zeller, D. Cissell, M. Metea, E. Adams, M. Higgins, K. H. Kim, E. Budzynski, L. Yang, Y. Liu, M. Butt, O. Danos, M. Fiscella, Characterization of AAV-mediated dorsal root ganglionopathy. *Mol. Ther. Methods Clin. Dev.* **24**, 342–354 (2022).
20. B. L. Davidson, C. S. Stein, J. A. Heth, I. Martins, R. M. Kotin, T. A. Derksen, J. Zabner, A. Ghodsi, J. A. Chiorini, Recombinant adeno-associated virus type 2, 4, and 5 vectors: Transduction of variant cell types and regions in the mammalian central nervous system. *Proc. Natl. Acad. Sci. U.S.A.* **97**, 3428–3432 (2000).
21. E. Hudry, J. Dashkoff, A. D. Roe, S. Takeda, R. M. Koffie, T. Hashimoto, M. Scheel, T. Spires-Jones, M. Arbel-Ornath, R. Betensky, B. L. Davidson, B. T. Hyman, Gene transfer of human Apoe isoforms results in differential modulation of amyloid deposition and neurotoxicity in mouse brain. *Sci. Transl. Med.* **5**, 212ra161 (2013).
22. D. E. Sleat, J. A. Wiseman, M. El-Banna, K. H. Kim, Q. Mao, S. Price, S. L. Macauley, R. L. Sidman, M. M. Shen, Q. Zhao, M. A. Passini, B. L. Davidson, G. R. Stewart, P. Lobel, A mouse model of classical late-infantile neuronal ceroid lipofuscinosis based on targeted disruption of the CLN2 gene results in a loss of tripeptidyl-peptidase I activity and progressive neurodegeneration. *J. Neurosci.* **24**, 9117–9126 (2004).
23. D. Sondhi, S. M. Kaminsky, N. R. Hackett, O. E. Pagovich, J. B. Rosenberg, B. P. De, A. Chen, B. Van de Graaf, J. G. Mezey, G. W. Mammen, D. Mancenido, F. Xu, B. Kosofsky, K. Yohay, S. Worgall, R. J. Kaner, M. Souwedaine, B. M. Greenwald, M. Kaplitt, J. P. Dyke, D. J. Ballon, L. A. Heier, S. Kiss, R. G. Crystal, Slowing late infantile Batten disease by direct brain parenchymal administration of a rh.10 adeno-associated virus expressing *CLN2*. *Sci. Transl. Med.* **12**, eabb5413 (2020).
24. Y. Matsuzaki, A. Konno, R. Mochizuki, Y. Shinohara, K. Nitta, Y. Okada, H. Hirai, Intravenous administration of the adeno-associated virus-PHP.B capsid fails to upregulate transduction efficiency in the marmoset brain. *Neurosci. Lett.* **665**, 182–188 (2018).

25. W. A. Liguore, J. S. Domire, D. Button, Y. Wang, B. D. Dufour, S. Srinivasan, J. L. McBride, AAV-PHP.B administration results in a differential pattern of CNS biodistribution in non-human primates compared with mice. *Mol. Ther.* **27**, 2018–2037 (2019).
26. D. E. Leib, Y. H. Chen, L. Tecedor, P. T. Ranum, M. S. Keiser, B. C. Lewandowski, E. M. Carrell, S. Arora, I. Huerta-Ocampo, X. Liu, B. L. Davidson, Optimized AAV capsids for diseases of the basal ganglia show robust potency and distribution in adult nonhuman primates. bioRxiv 592211 [Preprint] (2024). https://doi.org/10.1101/2024.05.02.592211.
27. N. Spassky, F. T. Merkle, N. Flames, A. D. Tramontin, J. M. Garcia-Verdugo, A. Alvarez-Buylla, Adult ependymal cells are postmitotic and are derived from radial glial cells during embryogenesis. *J. Neurosci.* **25**, 10–18 (2005).
28. A. Rodrigo Albors, G. A. Singer, E. Llorens-Bobadilla, J. Frisen, A. P. May, C. P. Ponting, K. G. Storey, An ependymal cell census identifies heterogeneous and ongoing cell maturation in the adult mouse spinal cord that changes dynamically on injury. *Dev. Cell* **58**, 239–255.e10 (2023).
29. C. Hinderer, P. Bell, C. H. Vite, J. P. Louboutin, R. Grant, E. Bote, H. Yu, B. Pukenas, R. Hurst, J. M. Wilson, Widespread gene transfer in the central nervous system of cynomolgus macaques following delivery of AAV9 into the cisterna magna. *Mol. Ther. Methods Clin. Dev.* **1**, 14051 (2014).
30. B. P. De, J. B. Rosenberg, N. Selvan, I. Wilson, N. Yusufzai, A. Greco, S. M. Kaminsky, L. A. Heier, R. J. Ricart Arbona, I. C. Miranda, S. Monette, A. Nair, R. Khanna, R. G. Crystal, D. Sondhi, Assessment of safety and biodistribution of AAVrh.10hCLN2 following intracisternal administration in nonhuman primates for the treatment of CLN2 Batten disease. *Hum. Gene Ther.* **34**, 905–916 (2023).
31. J. L. Cohen-Pfeffer, S. Gururangan, T. Lester, D. A. Lim, A. J. Shaywitz, M. Westphal, I. Slavc, Intracerebroventricular delivery as a safe, long-term route of drug administration. *Pediatr. Neurol.* **67**, 23–35 (2017).
32. M. Marino, M. G. Holt, AAV vector-mediated antibody delivery (A-MAD) in the central nervous system. *Front. Neurol.* **13**, 870799 (2022).
33. M. S. Goodwin, O. Sinyavskaya, F. Burg, V. O'Neal, C. Ceballos-Diaz, P. E. Cruz, J. Lewis, B. I. Giasson, P. Davies, T. E. Golde, Y. Levites, Anti-tau scFvs targeted to the cytoplasm or secretory pathway variably modify pathology and neurodegenerative phenotypes. *Mol. Ther.* **29**, 859–872 (2021).
34. M. Marino, L. Zhou, M. Y. Rincon, Z. Callaerts-Vegh, J. Verhaert, J. Wahis, E. Creemers, L. Yshii, K. Wierda, T. Saito, C. Marneffe, I. Voytyuk, Y. Wouters, M. Dewilde, S. I. Duque, C. Vincke, Y. Levites, T. E. Golde, T. C. Saido, S. Muyldermans, A. Liston, B. De Strooper, M. G. Holt, AAV-mediated delivery of an anti-BACE1 VHH alleviates pathology in an Alzheimer's disease model. *EMBO Mol. Med.* **14**, e09824 (2022).
35. D. G. T. Parambi, K. S. Alharbi, R. Kumar, S. Harilal, G. E. Batiha, N. Cruz-Martins, O. Magdy, A. Musa, D. S. Panda, B. Mathew, Gene therapy approach with an emphasis on growth factors: Theoretical and clinical outcomes in neurodegenerative diseases. *Mol. Neurobiol.* **59**, 191–233 (2022).
36. P. Bankhead, M. B. Loughrey, J. A. Fernandez, Y. Dombrowski, D. G. McArt, P. D. Dunne, S. McQuaid, R. T. Gray, L. J. Murray, H. G. Coleman, J. A. James, M. Salto-Tellez, P. W. Hamilton, QuPath: Open source software for digital pathology image analysis. *Sci. Rep.* **7**, 16878 (2017).
37. E. A. Waxman, L. V. Dungan, L. M. DeFlitch, J. P. Merchant, A. L. Gagne, E. M. Goldberg, D. L. French, Reproducible differentiation of human pluripotent stem cells into two-dimensional cortical neuron cultures with checkpoints for success. *Curr. Protoc.* **3**, e948 (2023).
38. E. Calabrese, A. Badea, C. L. Coe, G. R. Lubach, Y. Shi, M. A. Styner, G. A. Johnson, A diffusion tensor MRI atlas of the postmortem rhesus macaque brain. *Neuroimage* **117**, 408–416 (2015).

Acknowledgments: We acknowledge the Davidson lab for thoughtful discussions, A. Robbins for consultation on bioinformatic pipelines and for depictions of the ventricular system, P. Morris for animal husbandry and planning, and S. Masters for assistance with CSF acquisition. We thank M. McFadden and A. Mackiewicz and the entire Comparative Models Services Core and Department of Veterinary Resource staff at the Children's Hospital of Philadelphia (CHOP). **Funding:** This work was supported by the CHOP Research Institute and Latus Bio. **Author contributions:** Conception: L.T., Y.H.C., D.E.L., P.T.R., and B.L.D. Study design and execution: L.T., Y.H.C., D.E.L., P.T.R., M.S.K., B.C.L., E.L., E.M.C., I.H.-O., S.A., C.C., X.L., and B.L.D. Writing and editing: L.T., Y.H.C., D.E.L., P.T.R., E.M.C., B.C.L., and B.L.D. **Competing interests:** L.T., Y.H.C., D.E.L., P.T.R., M.S.K., and B.L.D. are founders of Latus Bio. D.E.L. and P.T.R. are employees of Latus Bio. B.L.D. has sponsored research or serves in an advisory role for Carbon Bio, Resilience, Roche, and Latus Bio. Relevant patents for this work are (i) PCT/US2024/013505, "Novel gene therapy construct for CLN2 disease" (B.L.D., P.T.R., M.S.K., Y.H.C., and L.T. are coauthors), (ii) PCT/US2024/052555, "AAV vectors for treatment of CLN2 disease" (B.L.D., P.T.R., M.S.K., Y.H.C., and L.T. are coauthors), and (iii) US 63/641,689, "Methods to increase transduction of ependyma cells in the brain" (L.T. and B.L.D. are coauthors). All other authors declare that they have no competing interests. **Data and materials availability:** All data associated with this study are present in the paper or the Supplementary Materials. All viruses and other materials are available upon request to the corresponding author through a material transfer agreement from the CHOP Office of Technology Transfer. Software used for capsid detection and performance analysis is available at DOI: 10.5281/zenodo.14851580 and https://github.com/DavidsonLabCHOP/DavidsonLab_AAVLibraryEnrichment.git.

Submitted 21 June 2024
Resubmitted 8 November 2024
Accepted 23 April 2025
Published 14 May 2025
10.1126/scitranslmed.adr2531